Hydrogen production from coke oven gas using pressure swing adsorption process − a mathematical modelling approach

Ramani, Balan; Van Der Stel, Jan; Jagers, Gerard; Buijs, Wim

DOI
10.1051/mattech/2023027

Publication date
2023

Document Version
Final published version

Published in
Materiaux et Techniques

Matériaux & Techniques **111**, 205 (2023)

https://doi.org/10.1051/mattech/2023027

Matériaux & Techniques

Available online at:
www.mattech-journal.org

Special Issue on 'The role of Hydrogen in the transition to a sustainable steelmaking process', edited by Ismael Matino and Valentina Colla

Regular Article

Hydrogen production from coke oven gas using pressure swing adsorption process – a mathematical modelling approach

Balan Ramani[1,2], Jan van der Stel[1], Gerard Jagers[1], and Wim Buijs[2,]

[1] Research and Development, Tata Steel Nederland Technology BV, Wenckebachstraat 1, Velsen-Noord, The Netherlands
[2] Faculty of Mechanical, Maritime and Materials Engineering, Delft University of Technology, Leeghwaterstraat 39, Delft, The Netherlands

Received: 16 May 2023 / Accepted: 6 September 2023

Abstract. Coal is playing a major role as a reductant and as an energy source in the present world steel production due to its low cost and widespread distribution around the world. At the same time, being the largest contributor to global CO_2 emissions, coal faces significant environmental challenges in terms of air pollution and global warming. Hydrogen is a promising alternative for coal in lowering the steel industry's CO_2 footprint, but the availability of green hydrogen is currently limited by its high production cost. This research study focuses on developing a pressure swing adsorption (PSA) technology that will allow for continued use of coal for a smooth transition towards green hydrogen-based steel production, by better utilisation of its by-product coke oven gas to produce high purity hydrogen. A generic, fast and robust simulation tool for simulating a variety of PSA processes considering both equilibrium and kinetic effects using a detailed non-isothermal and non-isobaric model is developed in the study. The adsorption equilibrium data required for the model are calculated from experimental results using the non-linear regression data fitting method. A series of rigorous parametric studies and breakthrough tests are performed using the developed mathematical model for better understanding of the effects of different factors on the PSA process performance. With the better understanding obtained from the above-mentioned parametric studies, the model is optimised by performing several simulation tests to achieve a high process performance in terms of purity and recovery of the H_2 product, productivity of the adsorbents and energy consumption for compression of gases. The optimised 14-step multi-bed PSA cycle developed in this study allows for an improved energy efficiency of coal usage by better utilisation of its by-product coke oven gas by converting it into valuable high purity (>99.999%) hydrogen product with a recovery of over 75%.

Keywords: Hydrogen / coke oven gas / gas separation / pressure swing adsorption / activated carbon / zeolite

1. Introduction

Coal plays a crucial role in the world's energy future for two reasons: First, it is the lowest-cost fossil source for base-load electricity generation. And second, in contrast to oil and natural gas, coal resources are widely distributed around the world spreading between developed and developing countries [1]. On the other hand, coal faces significant environmental challenges in terms of air pollution and global warming. In fact, coal is the largest contributor to global CO_2 emissions from energy use, and its share is projected to increase [2]. The solution to overcome global warming and environmental pollution issues lies not in a single technology but in more effective use of existing fuels and technologies, as well as wider adoption of alternative energy sources. Hence, focus should be on developing technologies that will allow continued operation of fossil fuels like coal in the transition towards clean energy future, while improving their energy efficiency by better utilization of their by-products and on reducing their environmental impact by CO_2 capture and utilization.

Steel industries are the largest energy consuming manufacturing sector in the world and coal being the cheapest form of fossil fuel, is their main source of reductant and energy. Hence, the CO_2 emissions associated with the steel industries are also very high and accounts for about 5–7% of the total anthropogenic CO_2 emissions [3]. Considering the fact that steel production is expected to increase especially in the developing countries, a significant increase in coal consumption and as well as CO_2 emissions are also expected to follow up. The steel industries have been committed to sustainability since 1960's and now the

* e-mail : balan.ramani@outlook.com

steel manufacturing processes through blast furnace route in many developed countries have reached considerably high levels of efficiency in terms of carbon use [3]. Global warming concerns have created the urge to look for alternate ways to improve energy efficiency and reduce greenhouse gases (GHG) emissions of the steel industries. During the coal pyrolysis process for preparing the coke to be used in blast furnace, coke oven gas (COG) is produced which is a point of high interest to enhance energy efficiency and reduce greenhouse gases emissions of the steel industry. Blast furnace cannot operate without coke which implies that the coke oven gas will also continue to be produced during the transition towards a green steel future.

Coke oven gas leaving the coke oven battery has a very complex composition. The gas is cooled down to separate tar, then passed through a series of scrubbing units to remove NH_3, H_2S and BTX (Benzene, Toluene and Xylene) as detailed in Ramani et al [4]. The presence of these minor components in the COG feed will affect the performance of the PSA process as they are strongly adsorbed to the adsorbent surface making it difficult to remove them from the adsorption bed. After the treatment process, the cleaned COG typically comprises of the following major gas components: H_2 (∼55–60%), CH_4 (∼23–27%), CO (∼5–8%), N_2 (∼3–6%), CO_2 (<2%), O_2 (<1%) along with other lighter hydrocarbons in small proportions [3].

COG is mainly used for its heating value (18 MJ/m^3) in the internal operations of steel making process and, in some cases, also for electricity production to meet internal power demands. The surplus gas is burnt off in torches and emitted to the atmosphere [3,5]. Current COG usage methods are energy inefficient and has a significant environmental impact in terms of large GHG emissions. COG containing ∼55–60% of H_2 is a high potential source of hydrogen which is regarded as a future clean energy source. In the future, centralized CO_2 emissions from the industries can be controlled using carbon capture technologies. But it is difficult to control the decentralized CO_2 emissions from automobiles. Hence, the mobility system needs to adopt Battery Electric Vehicles (BEVs) or Fuel Cell Electric Vehicles (FCEVs) which do not rely on fossil fuels and provide the long-term prospect of truly zero-emission. FCEVs have shorter refuelling time and much longer driving range as compared to BEVs making them more attractive for long-distance heavy-duty mobility applications [5]. The emerging hydrogen mobility market together with the upcoming hydrogen requirement for iron ore direct reduction processes might provide the opportunity for a possible new and efficient usage of COG.

Adsorption phenomenon is based on the physical binding of gas molecules to adsorbent surfaces. The binding force mainly depends on the nature of gas component, type of adsorbent material, partial pressure of the gas component in the mixture and operating temperature. Pressure swing adsorption (PSA) process work on the principle that adsorption occurs at high pressure and regeneration occurs at low pressure. They are generally equilibrium-controlled processes wherein different amount of adsorbate is adsorbed at different pressures during the cycle. Hydrogen being a highly volatile component with low polarity is weakly adsorbed as opposed to molecules such as CO, CO_2, N_2, CH_4 and other hydrocarbons present in coke oven gas. Hence the impurities present in COG can be adsorbed, thereby recovering high purity hydrogen [7]. Most of the PSA processes operate under adiabatic conditions where compressors provide the pressure required to achieve the separation. A PSA cycle can be very fast with a cycle time of generally few minutes. This leads to high productivity and small adsorbent beds reducing the capital cost. The design and operation of PSA cycles are very flexible allowing for quick adaptation to changes in feed composition and market demands [8].

The objectives of the study are to develop a generic tool for simulating dynamic pressure swing adsorption processes considering both equilibrium and kinetic effects, and to use the developed tool to optimise a multi-bed PSA cycle for producing high purity (>99.999%) hydrogen from coke oven gas with the best possible recovery.

2 Methodology

2.1 Selection of adsorbents

The industrial hydrogen purification by a PSA process involves adsorption bed made up of a series of layers of different adsorbents with different affinities for each impurity. Most of the literature studies about hydrogen production use activated carbon and zeolite 5A as adsorbents. Hydrogen for mobility applications require very high purity (>99.95%) and should eliminate carbon monoxide (CO) even in ppm levels (<0.2 ppm) in order to avoid CO poisoning [9]. The higher competition of carbon dioxide with carbon monoxide in zeolite 5A adsorbent leads to a lower carbon monoxide adsorption capacity and therefore a higher carbon monoxide concentration in the hydrogen product. In order to overcome this problem, a better suitable adsorbent like zeolite 13X could be used in place of zeolite 5A. But, the adsorption studies for hydrogen purification using zeolite 13X are less known than that of zeolite 5A. The literature study [10] shows that replacing zeolite 5A layer with zeolite 13X increases the hydrogen purity and recovery under the same operating conditions. Hence in this study, lithium-exchanged zeolite X (LiX) along with activated carbon are used as adsorbents for development of PSA process for hydrogen purification from coke oven gas.

2.2 Adsorption equilibrium

For the adsorption of pure gases, various single component models have been proposed to describe the adsorption loadings at different pressures and temperatures. Langmuir-Freundlich isotherm model is widely used to describe the physical adsorption of gases. The model is based on the kinetic principle that the rate of adsorption is equal to the rate of desorption from the surface. The mathematical

Table 1. Adsorption isotherm data for AC and LiX.

Species	q_{sat} (mol kg^{-1})		b_0 (bar^{-1})		ΔH (kJ mol^{-1})	
	AC	LiX	AC	LiX	AC	LiX
H_2	1.97	0.70	0.00872	0.01382	−2.63	−3.56
CH_4	4.47	3.21	0.00024	0.00080	−17.74	−14.84
CO	3.45	2.81	0.00075	0.01050	−13.28	−11.81
CO_2	6.85	5.13	0.00056	0.00010	−17.09	−28.49
N_2	3.44	2.39	0.00070	0.00038	−12.73	−17.14
O_2	4.68	5.74	0.00071	0.00055	−11.83	−8.94

form [11] of the isotherm model is

$$q^* = \frac{q_{sat} bP}{1 + bP}, \quad (1)$$

where

q^* −adsorbed phase equilibrium concentration of gas species, mol kg^{-1}

q_{sat} −saturation limit of adsorbed phase concentration of gas species, mol kg^{-1}

b −adsorption equilibrium constant, bar^{-1}

P -pressure, bar

Experimental adsorption isotherm data for pure gas species measured at different isotherm temperatures were taken from literature [12]. By performing non-linear regression analysis, the experimental data was fitted with the isotherm model equation to obtain the values of q_{sat} and b for each of the isotherm. For a useful description of the adsorption equilibrium data at different temperatures, it is necessary to have an isotherm model that is temperature dependent. The temperature dependence of the isotherm model for the equilibrium constant b may take the form [13],

$$b = b_0 \exp\left(\frac{-\Delta H}{RT}\right), \quad (2)$$

where

b_0 −pre-exponential factor, $\left(= f\left(\frac{\Delta S}{R}\right)\right)$ bar^{-1}

R −universal gas constant, (=8.314) J mol^{-1} K^{-1}

ΔH -enthalpy change on adsorption, J mol^{-1}

ΔS −entropy change on adsorption, J mol^{-1} K^{-1}

T -temperature, K

Van't Hoff graphs are plotted between lnb and $\frac{1}{T}$ to calculate ΔH and b_0 of the pure gas species. The resulting values of adsorption isotherm data for activated carbon (AC) and zeolite LiX are summarised in Table 1.

For the adsorption of multicomponent gas mixtures, the single component models can be extended to include the influence of other components on the adsorption behaviour of each individual component [13] with the possibilities of having competitive or non-competitive adsorption with/without the dissociation of gases (chemisorption). The total adsorption capacity includes the combined effects of competitive adsorption or non-competitive adsorption and dissociation of gases. Since the focus is on physisorption, the dissociation of gases i.e., chemisorption effects are not considered. In general, each adsorption site can hold at most one molecule of gas species. Hence the different gas components present in the feed compete for the same site of adsorption. The adsorption capacity of component i in a mixture of N components is thus determined via the following competitive adsorption equation:

$$q_i^* = \frac{q_{sat_i} b_i P_i}{1 + \sum_N^{j=1} b_j P_j}. \quad (3)$$

This adsorption equilibrium model described above using the extended Langmuir-Freundlich isotherm model is used to estimate the adsorptive capacity of coke oven gas (COG) components on different adsorbents. The properties of clean coke oven gas feed to PSA system used in this study is shown in Table 2. In case any minor components are still present in trace amount in the COG even after the treatment process, an additional adsorption column should be placed before the actual PSA installation, in order to ensure complete removal of minor components from COG before being fed to the hydrogen sequestration PSA system.

2.3 Model equations

Process simulation has become an essential part of a process engineer's work ever since the evolution of modern processors capable of computing complex equations in a reasonable amount of time. Adsorption processes are dynamic in nature unlike the steady state behaviour exhibited by other major separation processes like distillation and absorption. Hence, analytical solutions that work well with the above-mentioned steady state separation technologies are not sufficient for adsorption processes. This impedes the development of a design method for adsorption process as those used in the steady state technologies.

Numerical methods have become increasingly popular and feasible with the modern powerful computers. Simulators developed for pressure swing adsorption (PSA) systems require complex boundary conditions that allows quick outcome predictions from changes in process conditions like pressure, temperature and composition etc.

Table 2. Properties of COG feed.

Pressure P (bar)	1
Temperature T (K)	298.15
Flow rate F_m (mol s^{-1})	160
H_2 (vol.%)	64.3
CH_4 (vol.%)	25.7
CO (vol.%)	5.9
CO_2 (vol.%)	1.3
N_2 (vol.%)	2.6
O_2 (vol.%)	0.2

and make corresponding adjustments. The simulation also reduces capital investment in the preliminary design of a novel process cycle. Hence, a detailed model put into an accurate simulator allows a process engineer to optimize a process as complex as PSA rapidly while inspiring industrial confidence at the same time [7].

A pressure swing adsorption bed model must take into account the simultaneous mass, heat and momentum balances in the bulk gas flow, the transport and thermophysical properties of the gas mixture and a set of boundary conditions for the input and output from the bed and the interface between the bulk gas and particle surface [14–17]. The following assumptions are used to derive the model equations [18].

- The gas components are following ideal gas behaviour.
- The gas flow follows the axially dispersed plug flow model.
- The mass transfer rate follows the linear driving force (LDF) model.
- The frictional pressure drop in axial direction follows Darcy's law.
- The pressure, temperature and concentration gradients in the radial direction are negligible.
- The gas and the adsorbent are in a state of thermal equilibrium.
- Heat transfer occurs along the column wall whose outer surface is maintained at a constant temperature.
- The adsorbent properties and bed porosity are uniform along the column.

The component mass balance equation is given by

$$\varepsilon\frac{\partial c_i}{\partial t}+(1-\varepsilon)\varepsilon_p\frac{\partial c_i}{\partial t}\varepsilon\frac{\partial}{\partial z}\left[-D_{ax}\frac{\partial c_i}{\partial z}+c_i v\right]+(1-\varepsilon)\frac{\partial q_i}{\partial t}=0. \tag{4}$$

The total mass balance equation is given by

$$\varepsilon\frac{\partial\rho_g}{\partial t}+\varepsilon\frac{\partial}{\partial z}\left(\rho_g v\right)+(1-\varepsilon)\left(\varepsilon_p\frac{\partial\rho_g}{\partial t}+\sum_{i=1}^{n_{comp}}\frac{\partial q_i}{\partial t}\right)=0. \tag{5}$$

The rate of adsorption into solid phase considering LDF model is given by

$$\frac{\partial q_i}{\partial t}=k_i\left(q_i^*-q_i\right). \tag{6}$$

The energy balance for solid and gas phase is given by

$$\left[\varepsilon\rho_g C_{pg}+(1-\varepsilon)\varepsilon_p\rho_g C_{pg}+(1-\varepsilon)\rho_s C_{ps}\right]\frac{\partial T}{\partial t}-(1-\varepsilon)\sum_{i=1}^{n_{comp}}\left((-\Delta H_i)\frac{\partial q_i}{\partial t}\right)-\lambda_{ax}\frac{\partial^2 T}{\partial z^2}+\varepsilon\rho_g C_{pg}\frac{\partial}{\partial z}(vT)+\frac{2h_{in}}{r_{in}}(T-T_w)=0. \tag{7}$$

The energy balance for walls is given by

$$\rho_w C_{pw}\frac{\partial T_w}{\partial t}-\lambda_w\frac{\partial^2 T_w}{\partial z^2}-\frac{2r_{in}h_{in}}{r_{out}^2-r_{in}^2}(T-T_w)+\frac{2r_{out}h_{out}}{r_{out}^2-r_{in}^2}(T_w-T_a)=0. \tag{8}$$

According to Darcy's law, pressure drop along the length of the column is given by

$$\frac{\partial P}{\partial z}=-\frac{150}{4}\frac{1}{r_p^2}\left(\frac{1-\varepsilon}{\varepsilon}\right)^2\mu v. \tag{9}$$

The interstitial velocity is evaluated by rearranging equation (9)

$$v=\left(-\frac{\partial P}{\partial z}\right)\frac{4}{150}r_p^2\left(\frac{\varepsilon}{1-\varepsilon}\right)^2\frac{1}{\mu}. \tag{10}$$

Axial concentration and temperature gradients always exist in packed beds. Hence, a diffusive mass and heat transfer will always occur and tend to degrade the performance of the process. Therefore, an accurate prediction of mass and thermal axial dispersion coefficients is very important for detailed modelling of the flow through the packed bed. Wakao developed one of the most widely used coefficients [14]:

$$D_{ax}=\frac{D_m}{\varepsilon}(20+0.5ScRe), \tag{11}$$

$$\lambda_{ax}=\lambda_g(7+0.5PrRe), \tag{12}$$

where

Schmidt number, $Sc=\frac{\mu}{\rho_g D_m}$

Reynolds number, $Re=\frac{\rho_g\varepsilon u d_p}{\mu}$

Prandtl number, $Pr=\frac{C_{pg}\mu}{\lambda_g}$

The molecular diffusivity is calculated using Chapman-Enskog equation [12,20].

$$D_{m,i} = 0.0018583 \frac{T^{\frac{3}{2}}\left(\frac{1}{MW_i}\right)^{\frac{1}{2}}}{P\sigma^2\Omega}, \tag{13}$$

where the Lennard Jones potential energy function [20,21] is given by

$$\sigma = \frac{\sigma_1 + \sigma_2 + \sigma_3 + \ldots + \sigma_n}{n},$$

$$\xi = \sqrt{\xi_1 \xi_2 \ldots \xi_n},$$

and the collision integral is a function given by

$$\Omega = f\left(\frac{k_B T}{\xi}\right).$$

The Knudsen diffusivity [11] is calculated using the following equation.

$$D_{k,i} = 9.7 * 10^3 r_{pore} \sqrt{\frac{T}{MW_i}}. \tag{14}$$

The effective diffusivity is given by

$$D_{e,i} = \frac{\varepsilon_p}{\tau} \frac{1}{\left(\frac{1}{D_{m,i}} + \frac{1}{D_{k,i}}\right)}. \tag{15}$$

The mass transfer coefficient is calculated using the effective diffusivity [11] using the following formula

$$k_i = \frac{15 D_{e,i}}{r_p^2}. \tag{16}$$

In order to rigorously optimize cyclic adsorption processes using detailed models, robust numerical simulation techniques are necessary. The scheme should be fast and robust enough to handle stiff problems, while capturing the process dynamics and performance accurately. Due to the nature of the conservation equations, sharp fronts of concentration and temperature may propagate along the adsorption bed. Assuring the accuracy and stability of the model in such situations is challenging, especially when dealing with highly non-linear isotherms. Finite volume methods (FVM) rely on integration to give a more fundamental interpretation of mass, energy or momentum fluxes between interfaces, thereby the mass, energy and momentum conservations are rigorous. In this work, finite volume numerical method is thus chosen for the spatial discretisation. In cases where sharp discontinuities propagate in the system, weighted essentially non-oscillatory (WENO) method has successfully been implemented with the FVM framework to reduce non-physical oscillations around discontinuities, while still capturing the smooth portion of the solution.

2.4 Boundary conditions

The solution of the above equations requires proper initial and boundary conditions. Ideal initial condition assumes the column to be saturated with a known gas at particular pressure and temperature.

In Table 3, the boundary conditions for all the steps in the PSA cycle are generalized into three basic types as follows:

- Open-Open: In this type of flow, both the feed and product ends are open.
- Open-Closed: In this type of flow, the feed end is open while the product end is closed.
- Closed-Open: In this type of flow, the feed end is closed while the product end is open.

A combination of Dirichlet (the value of boundary point is specified) and Neumann (the derivative of boundary is specified) boundary conditions are used for close prediction of the behaviour of the column at its ends during different steps [18,22]. If the flow across the column is in opposite direction, then the boundary conditions are reversed.

2.5 Mass and Energy Balance error

The accuracy of the model is checked by calculating mass and energy balance errors. The larger the number of discretisation volumes (N) the better the accuracy is. But large number of discretisation volumes, require high computational time. Hence, a balance between accuracy and computational time has to be made. It was found that for $N \geq 50$ the accuracy is sufficiently high.

The mass balance error can be calculated from the following equation:

$$mass_{balance} = \frac{mass_{in} - (mass_{out} + mass_{acc})}{mass}, \tag{17}$$

where

$$mass_{in} = \varepsilon A \int_0^{t_{final}} (\rho_g v)|_{z=0} dt,$$

$$mass_{out} = \varepsilon A \int_0^{t_{final}} (\rho_g v)|_{z=L} dt,$$

$$mass_{acc} = mass_{acc,solid} + mass_{acc,fluid},$$

$$mass_{acc,fluid} = \left[\varepsilon A \int_0^L \left(\rho_g|_{t=t_{final}} - \rho_g|_{t=0}\right) dz\right] + \left[(1-\varepsilon)\varepsilon_p A \int_0^L \left(\rho_g|_{t=t_{final}} - \rho_g|_{t=0}\right) dz\right],$$

$$mass_{acc,solid} = \left[(1-\varepsilon) A \int_0^L \left(\Sigma q_i|_{t=t_{final}} - \Sigma q_i|_{t=0}\right) dz\right],$$

$$\text{mass} = \frac{\text{mass}_{\text{in}} + \text{mass}_{\text{out}}}{2}.$$

In addition to the mass balance error, the heat balance error can be calculated from the following equation:

$$\text{heat}_{\text{balance}} = \frac{\text{heat}_{\text{in}} + \text{heat}_{\text{gen}} - (\text{heat}_{\text{out}} + \text{heat}_{\text{acc}})}{\text{heat}}, \quad (18)$$

where

$$\text{heat}_{\text{in}} = \varepsilon A C_{\text{pg}} \int_0^{t_{\text{final}}} (T\rho_g v)|_{z=0} dt,$$

$$\text{heat}_{\text{out}} = \varepsilon A C_{\text{pg}} \int_0^{t_{\text{final}}} (T\rho_g v)|_{z=L} dt,$$

$$\text{heat}_{\text{gen}} = \left[(1-\varepsilon)A \int_0^{L} \left(\Sigma \Delta H_i q_i|_{t=t_{\text{final}}} - \Sigma \Delta H_i q_i|_{t=0}\right) dz\right],$$

$$\text{heat}_{\text{acc}} = \text{heat}_{\text{acc,solid}} + \text{heat}_{\text{acc,fluid}},$$

$$\text{heat}_{\text{acc,solid}} = \left[(1-\varepsilon) A C_{\text{ps}} \rho_s \int_0^{L} \left(T|_{t=t_{\text{final}}} - T|_{t=0}\right) dz\right] + \left[A_w C_{\text{pw}} \rho_w \int_0^{L} \left(T_w|_{t=t_{\text{final}}} - T_w|_{t=0}\right) dz\right],$$

$$\text{heat}_{\text{acc,fluid}} = \left[\varepsilon A C_{\text{pg}} \int_0^{L} \left(T\rho_g|_{t=t_{\text{final}}} - T\rho_g|_{t=0}\right) dz\right] + \left[(1-\varepsilon)\varepsilon_p A C_{\text{pg}} \int_0^{L} \left(T\rho_g|_{t=t_{\text{final}}} - T\rho_g|_{t=0}\right) dz\right]$$

$$\text{heat} = \frac{\text{heat}_{\text{in}} + \text{heat}_{\text{out}}}{2}.$$

2.6 Process Performance

The performance of the PSA process is evaluated by considering the following parametric values at CSS, defined by

$$\text{Purity}\% = \frac{\text{mass}_{\text{out,H}_2}|_{\text{ads}}}{\text{mass}_{\text{out}}|_{\text{ads}}} * 100,$$

$$\text{Recovery}\% = \frac{\text{mass}_{\text{out,H}_2}|_{\text{ads}}}{\text{mass}_{\text{in,H}_2}|_{\text{ads}} + \text{mass}_{\text{in,H}_2}|_{\text{rep}}} * 100,$$

$$\text{Productivity} = \frac{\text{mass}_{\text{out,H}_2}|_{\text{ads}}}{\text{adsorbentvolume} * \text{cycletime}},$$

$$E_T = \frac{(E_{\text{ads}})}{\text{Mass of H}_2 \text{ in the raffinate stream per cycle}},$$

where

$$E_{\text{ads}} = \frac{1}{\eta} \varepsilon A \left(\frac{\gamma}{\gamma - 1}\right) \int_0^{t_{\text{ads}}} vP|_{z=0} \left[\left(\frac{P|_{z=0}}{P_{\text{COG}}}\right)^{\frac{\gamma-1}{\gamma}} - 1\right] dt.$$

An extensive parameter study was performed to understand the effects of various factors on the performance of the multi-bed PSA process developed for high purity hydrogen production from coke oven gas. Aiming for hydrogen purity greater than 99.999% with the best possible recovery, simulations were run by varying the parameters such as purge to feed ratio, feed temperature, pressure, particle size, number of pressure equalisations, duration of different steps, feed flow rate, flow direction, carbon to zeolite ratio. Each of the simulation yields a cyclic steady state with H_2 purity and recovery values. Model validation and parametric study results can be found in [4]. Through the parameter studies, a better understanding of the effects of different parameters on the performance of PSA cycle is achieved. With the knowledge gained from parametric studies, several optimisations are performed using the combined effects of different parameters in order to obtain the best possible performance for the PSA process and their results are presented in the following section.

3 Results and discussion

A set of four two-columned pressure swing adsorption cycle with counter-current purge and depressurisation with one pressure equalisation step is used for producing high purity hydrogen from coke oven gas. The step configuration of the optimised PSA cycle is shown in Figure 1.

The pressurised coke oven gas feed enters the carbon (AC) column wherein the adsorption of the impurities takes place in the bed. The hydrogen enriched outflow of the carbon bed is connected to the feed end of zeolite (13X) column in which the adsorption process continues wherein high purity hydrogen with desired feed quality requirements for mobility applications is obtained at the product end. After the adsorption step, the feed end of carbon column is closed leaving the product end open. Evacuation takes place in the bed and hydrogen being the weakly adsorbed species comes out of the column first which is passed subsequently through the zeolite column and high purity hydrogen is collected at the zeolite column's product end. After the evacuation step is over, the feed end of zeolite column is also closed. This step is followed by the depressurising pressure equalisation step in which the

Table 3. Generalised Boundary Conditions for different steps of PSA cycle.

Step Type	z=0	z=L
Open-Open (Adsorption / Purge)	$\frac{\partial y_i}{\partial z}\|_{z=0} = y_{i,feed}$	$\frac{\partial y_i}{\partial z}\|_{z=L} = 0$
	$\frac{\partial T}{\partial z}\|_{z=0} = T_{feed}$	$\frac{\partial T}{\partial z}\|_{z=L} = 0$
	$T_w\|_{z=0} = T_a$	$T_w\|_{z=L} = T_a$
	$v\|_{z=0} = v_{feed}$	$\frac{\partial v}{\partial z}\|_{z=L} = 0$
Open-Closed (Repressurization / Pressure Equalisation ↑)	$\frac{\partial y_i}{\partial z}\|_{z=0} = y_{i,feed}$	$\frac{\partial y_i}{\partial z}\|_{z=L} = 0$
	$\frac{\partial T}{\partial z}\|_{z=0} = T_{feed}$	$\frac{\partial T}{\partial z}\|_{z=L} = 0$
	$T_w\|_{z=0} = T_a$	$T_w\|_{z=L} = T_a$
	$v\|_{z=0} = v_{feed}$	$v\|_{z=L} = 0$
Closed-Open (Evacuation / Blowdown / Pressure Equalisation ↓)	$\frac{\partial y_i}{\partial z}\|_{z=0} = 0$	$\frac{\partial y_i}{\partial z}\|_{z=L} = 0$
	$\frac{\partial T}{\partial z}\|_{z=0} = 0$	$\frac{\partial T}{\partial z}\|_{z=L} = 0$
	$T_w\|_{z=0} = T_a$	$T_w\|_{z=L} = T_a$
	$v\|_{z=0} = 0$	$\frac{\partial v}{\partial z}\|_{z=L} = 0$

product ends of each of carbon and zeolite columns are connected to the product ends of their counterpart columns respectively which are in their pressurising pressure equalisation step. The gas components move from the high pressure to low pressure columns resulting in pressurisation of the low-pressure columns. After the pressure equalisation step is over, the columns are enriched with CH_4 which are blown down through the product ends during the depressurisation step to atmospheric pressure. After depressurisation, still some impurities remain in the bed due to their equilibrium condition. Now, the feed ends of both the columns are open. A part of the H_2 product is used as purge stream and passed through the product end of the zeolite column and the outflow from the zeolite feed end enters the product end of carbon column. During this step, the remaining impurities present in the bed are pushed out of the columns and collected at the feed end of carbon column. At the end of purge step, the impurities are removed from the beds and thus the columns are regenerated. The purge step is followed by the pressurising pressure equalisation step in which the high-pressure gas components from the depressurising columns are passed through the product ends of the columns with the feed ends closed resulting in pressurisation of the columns. The repressurisation step follows the pressure equalisation step in which a part of high purity H_2 product is used to further pressurise the columns to make the beds ready for the next cycle of adsorption.

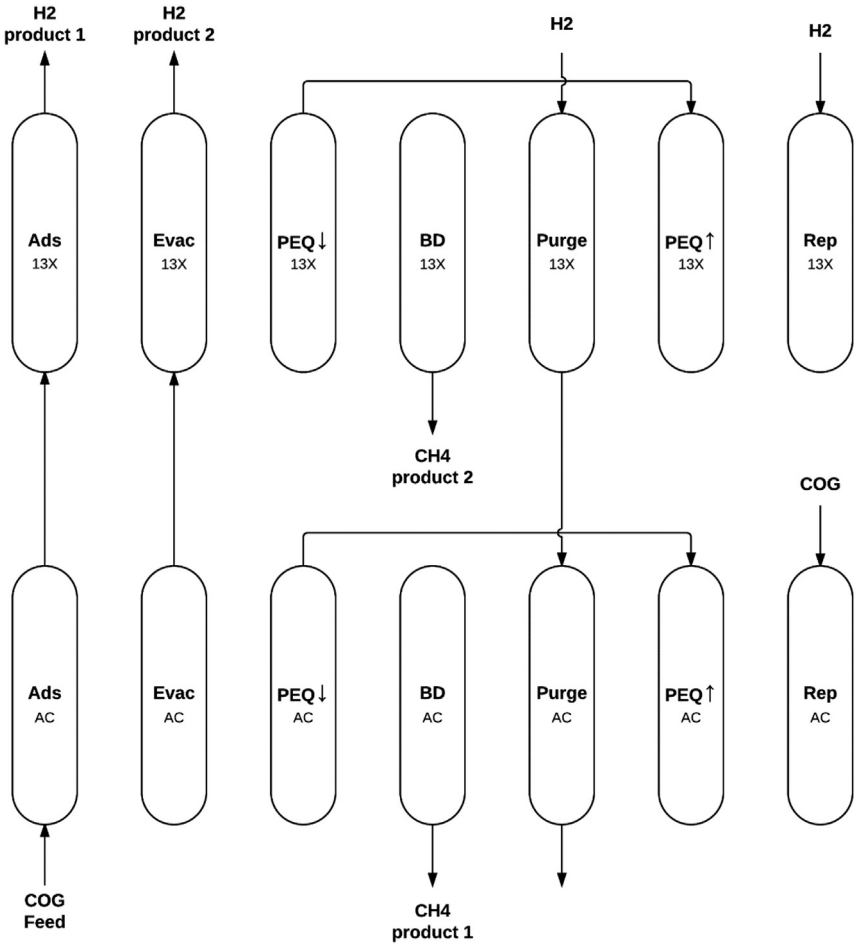

Fig. 1. Step configuration of a four-column PSA cycle (Ads −adsorption; Evac −evacuation; PEQ↓ −pressurising pressure equalisation; BD −blowdown; PEQ↓ −pressurising pressure equalisation; Rep −Depressurisation).

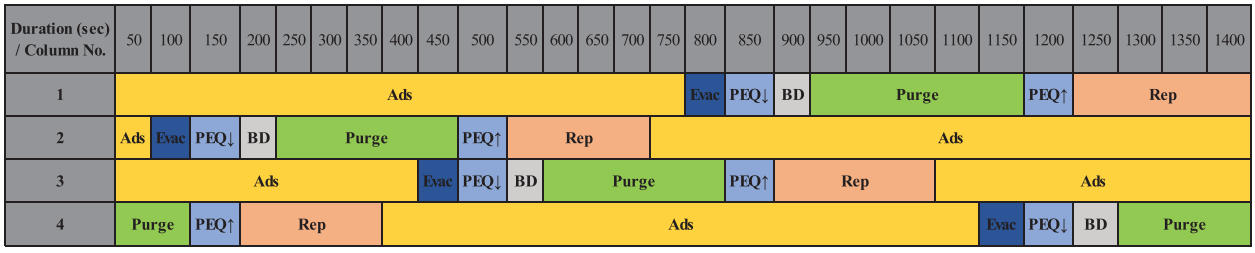

Fig. 2. Cycle timing diagram of 4-columns (each for AC and 13X) for the 14 step PSA cycle with counter-current H_2 purge.

The sequence of steps was repeated until the simulation reaches a cyclic steady state (CSS). Strictly considering, a CSS condition is reached only when there is no change in the column profiles of all the state variables after each step for two consecutive cycles. To check whether the simulation reached its cyclic steady state or not, the performance parameters i.e., the purity and recovery of H_2 product for five consecutive cycles were compared. It was considered that a CCS condition is reached when the difference of the purity and recovery of H_2 for the five consecutive cycles were both less than 10^{-6}.

Cycle timing for the 4 columns in parallel for each of carbon and zeolite beds is shown in Figure 2 depicting the relative duration for each step. At every instant of time, there is at least one column in the adsorption step thereby making the product outflow continuous. Also, the depressurising and pressurising pressure equalisation steps must be connected in time thereby ensuring proper pressure transfer from high pressure to low pressure columns. Numerically, a single column is simulated in time while the connecting steps are stored.

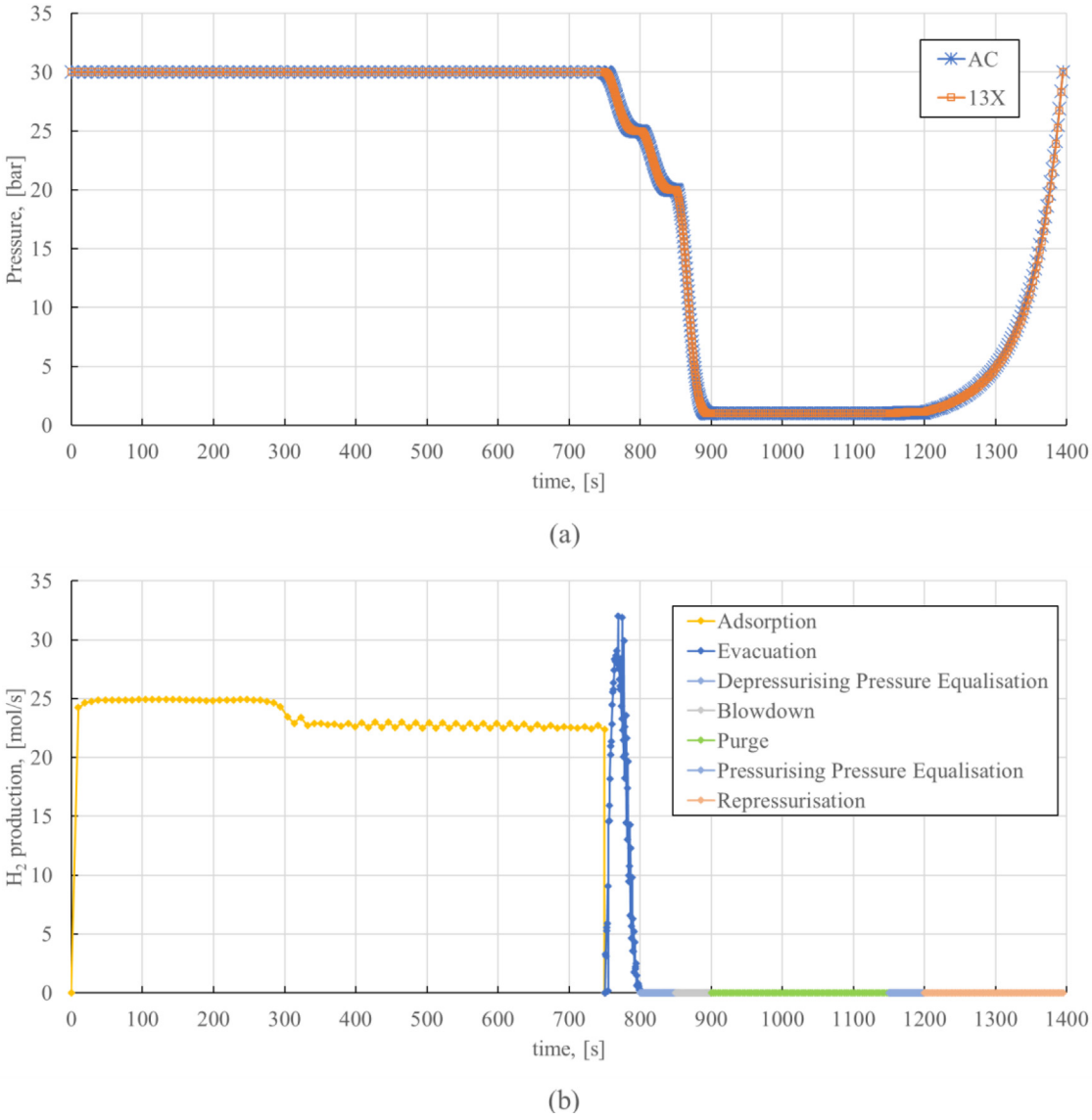

Fig. 3. (a) Pressure profiles at the outlet end of the carbon (AC) and zeolite (13X) columns, and (b) Hydrogen production over a cycle at the steady state condition of the PSA unit.

The pressure profile at the outlet end of the carbon and zeolite beds, and the hydrogen production rate over a cycle of a single column of the PSA unit at the cyclic steady state condition are shown in Figure 3. It can be seen that hydrogen is produced from a single column steadily at a rate of around 24 mol/s during the adsorption step (at 30 bar) for a duration of 750 s. At the end of the adsorption step of the first column, the next and subsequent columns start with their adsorption step, thereby resulting in the continuous production of hydrogen.

Pareto plots are made for three different feed pressures (P_H) by varying the feed flow rate as shown in Figure 4. Moving from one point on any Pareto curve to another on the same curve results in the improvement of one performance parameter, either purity or recovery at the expense of the other. It can be seen that as we move along the right of a parity curve, the purity of the product increases with the compensation in product recovery. Also, from the Pareto plots for three different feed pressures, it can be visualised that as the feed pressure increases a desired purity could be achieved with much better recovery than that of a lower feed pressure.

Also, the Pareto plots could be used as a tool for sensitivity analysis. It shows how the outcome of simulation varies with small deviations of various boundary conditions. In this case, the analysis is performed by slightly varying the feed pressure and feed flow rate to observe their effects on the purity and recovery of the product. It can be seen that the model accurately captures the small changes in boundary conditions during the simulation of the process to give precise results of their effects on process performance.

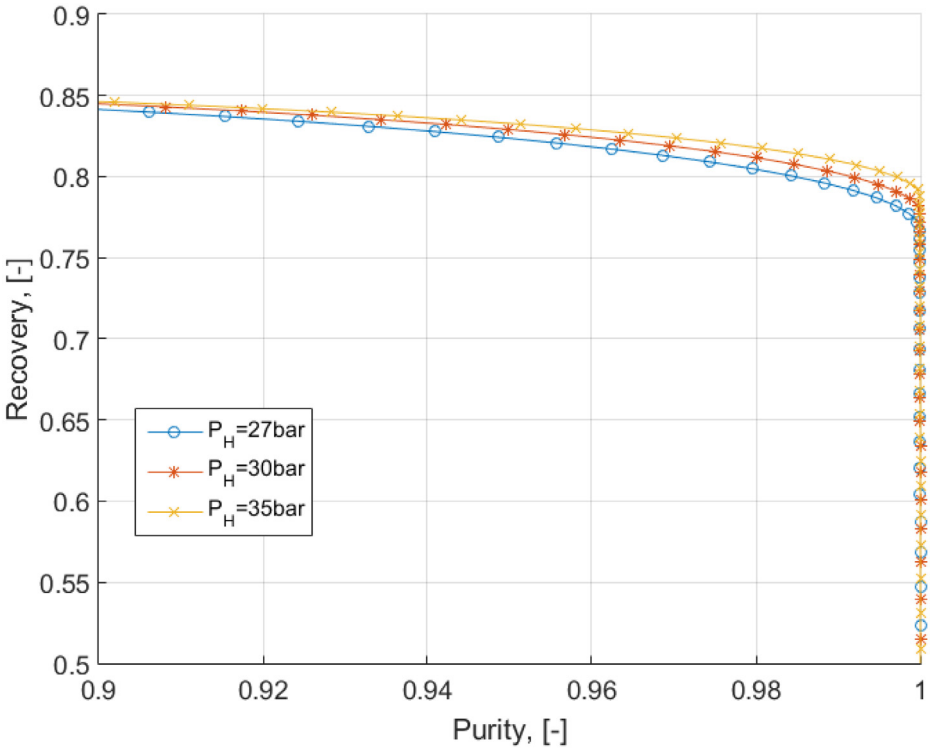

Fig. 4. Pareto curves for the optimisation problem of simultaneously increasing purity and recovery.

A comparison of hydrogen purity and recovery of the PSA system with changes in purge-to-feed ratio is shown in Figure 5. It can be seen that as the purge-to-feed ratio increases, the purity of the product increases with a decrease in product recovery. At the P/F ratio of 0.18, the hydrogen product reaches the desired purity of 99.999+% with a recovery of 78%. Further increase of the P/F ratio results in unwanted loss of product recovery which should be avoided for better overall performance of the process.

The optimised values of different parameters used in improving the performance of the PSA simulation process are summarised in Table 4.

Gas phase concentrations in the carbon and zeolite beds at the start and end time of each step during the PSA cycle is shown in Figures 6 and 7 respectively.

Variation of gas concentration profile at the outlet of the column as a function of time for each step of the PSA cycle is shown in Figure 8. It can be seen from the gas concentration profile of Figure 7 at the end of adsorption step of zeolite column that the adsorption step was just stopped before the H_2 wavefront reaches the end of the column. This ensures that the hydrogen product at the outlet end is still pure and free from impurities as shown in Figure 8. Further extension of adsorption step timing dilutes the hydrogen product with impurities which should be avoided.

Also, it can be seen from the outflow of step 4 of Figure 8 that when the pressure is decreased during the evacuation step, hydrogen being the weakly bonded gas component is the first to get desorbed from the bed which could be collected thereby increasing product recovery. During depressurising pressure equalisation step, the remaining hydrogen present in the bed is transferred to the low-pressure column.

Now, the column rich with CH_4 mixture is blown down as bottom product as shown in Figure 8. Variation of adsorbate loading at the end of each step of the PSA cycle is shown in Figure 9. It can be seen from the adsorbate loading at the end of step 7 and step 8 of Figure 9 that some gas components remain adsorbed in the bed after blowdown step. A part of H_2 product is used to purge out the remaining gas components present in the bed.

After the purging step, the beds are better regenerated and are repressurised with H_2 product making them ready for next cycle of adsorption. It can be observed from step 13 and step 14 of Figures 7 that after depressurisation step, both the bulk phase gas concentration in the bed and the adsorbate loading are free from impurities thereby ensuring effective adsorption of impurities during the next cycle of adsorption.

The concentration of impurities present in the hydrogen product are compared with the desired concentration levels for mobility applications [23,24], and are found to be well within the allowable concentration levels as shown in Table 5.

Apart from the production of high purity hydrogen which is the desired product, the PSA process also produces two other valuable streams of methane rich product from the blowdown steps and an outlet purge stream whose composition is similar to that of the feed

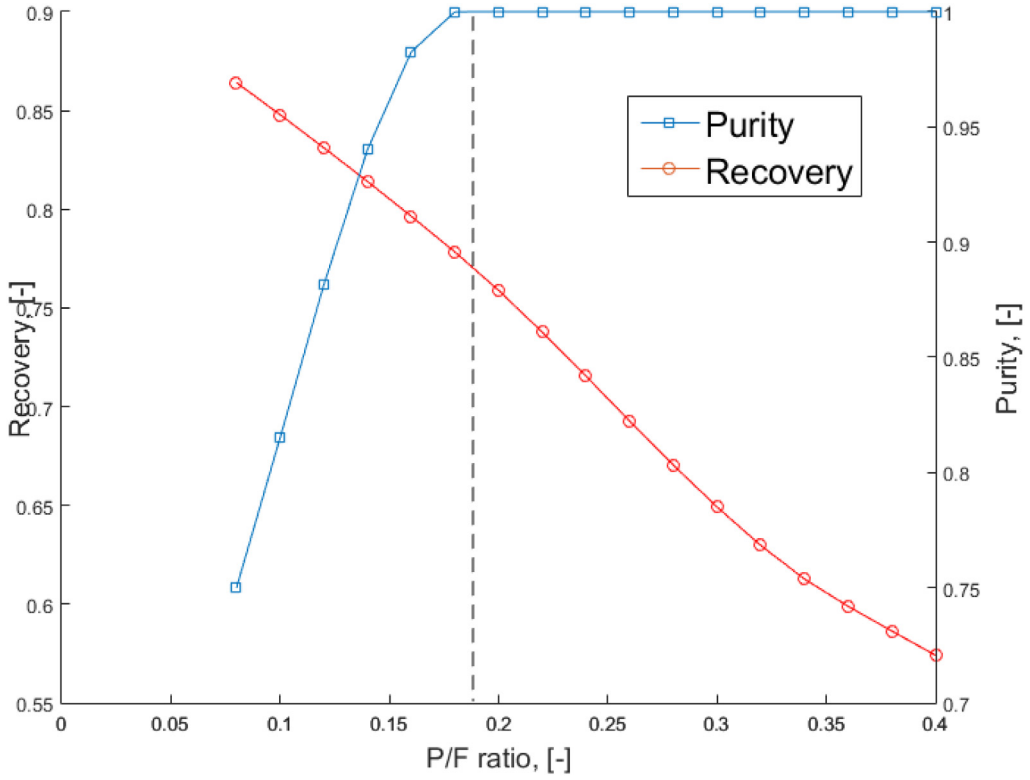

Fig. 5. Comparison of hydrogen purity and recovery of the PSA system with different purge-to feed ratio.

Table 4. Optimised values of the parameters used in PSA simulation.

Parameter	Value
Operating conditions:	
Feed Pressure, P_H (bar)	30
Blowdown Pressure, P_L (bar)	1
Equalisation Pressure, P_{EQ} (bar)	20
Evacuation Pressure, P_{Evac} (bar)	25
Feed Temperature, T (K)	298
Feed flow rate, $F_{m,feed}$ ($mol\,s^{-1}$)	30
Purge flow rate, $F_{m,purge}$ ($mol\,s^{-1}$)	10
Repress flow rate, $F_{m,repress}$ ($mol\,s^{-1}$)	16
Purge-to-Feed ratio, P/F (−)	0.18
Bed Properties:	
Total column length, L (m)	15
Inner column radius, r_{in} (m)	0.350
Outer column radius, r_{out} (m)	0.355
Carbon-to-Zeolite ratio, AZ (−)	0.5
Particle radius, r_p (mm)	2
Duration of each step:	
Adsorption time, t_{Ads} (s)	750
Evacuation time, t_{Evac} (s)	50
Equalisation time, t_{PEQ} (s)	50
Blowdown time, t_{BD} (s)	50
Purge time, t_{purge} (s)	250
Repress time, t_{Rep} (s)	200

COG gas. The outlet purge stream can hence be mixed with the COG feed to be used as feed stream to the PSA cycle thereby improving the overall product recovery to 86%. The heating value of the blowdown streams are quite good on volume basis due to their rich methane content and hence could be used to partially displace natural gas usage in the internal operations of steel making process. The operating conditions of the different streams involved in the PSA process are summarised in Table 6.

The developed PSA system operates with 8 columns in total, four each for carbon and zeolite beds. The specifications for each of the carbon and zeolite columns are in accordance with technical feasibility as summarised in Table 7.

The resulting performance parameters for the optimised PSA cycle for producing high purity hydrogen product from coke oven gas are calculated and the results are summarised in Table 8. It should be noted that this high purity of hydrogen product (99.999+%) is required for mobility application. If the hydrogen is to be used for internal steelmaking applications as for direct reduction or annealing processes, such a high purity is not necessary. The desired concentration levels of impurities in the hydrogen gas used for direct reduction of iron ore is not well-defined, but from literature it can be seen that a hydrogen purity of 95 to 98% is targeted for this application [25,26]. This implies that an additional 2 to

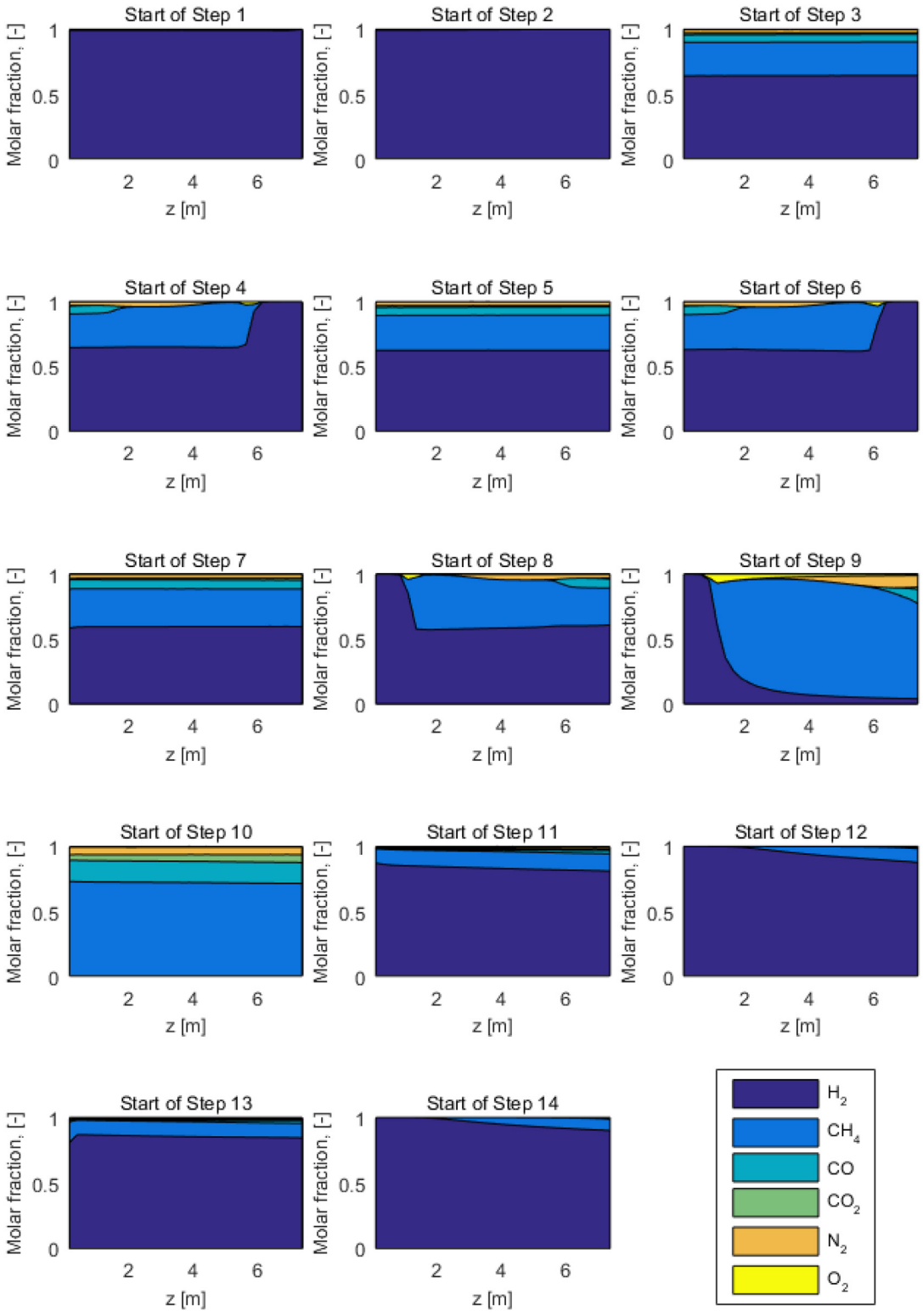

Fig. 6. Gas phase concentrations in the bed at the start of each step during the PSA cycle. Steps: (1) AC Adsorption; (2) 13X Adsorption; (3) AC Evacuation; (4) 13X Evacuation; (5) AC Depressurising Pressure Equalisation; (6) 13X Depressurising Pressure Equalisation; (7) AC Blowdown; (8) 13X Blowdown; (9) 13X Purge; (10) AC Purge; (11) 13X Pressurising Pressure Equalisation; (12) AC Pressurising Pressure Equalisation; (13) AC Depressurisation; (14) 13X Depressurisation.

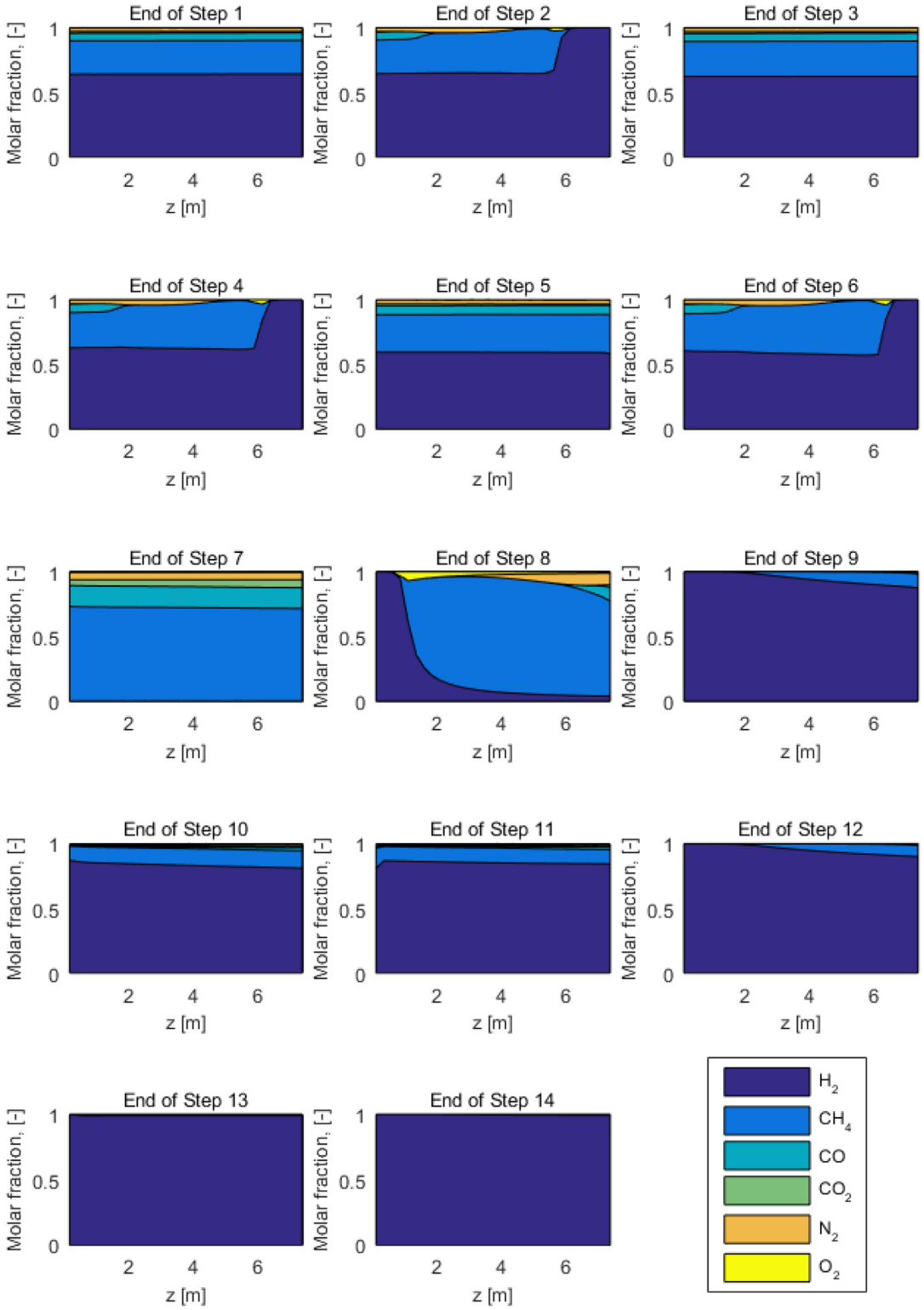

Fig. 7. Gas phase concentrations in the bed at the end of each step during the PSA cycle. Steps: (1) AC Adsorption; (2) 13X Adsorption; (3) AC Evacuation; (4) 13X Evacuation; (5) AC Depressurising Pressure Equalisation; (6) 13X Depressurising Pressure Equalisation; (7) AC Blowdown; (8) 13X Blowdown; (9) 13X Purge; (10) AC Purge; (11) 13X Pressurising Pressure Equalisation; (12) AC Pressurising Pressure Equalisation; (13) AC Depressurisation; (14) 13X Depressurisation.

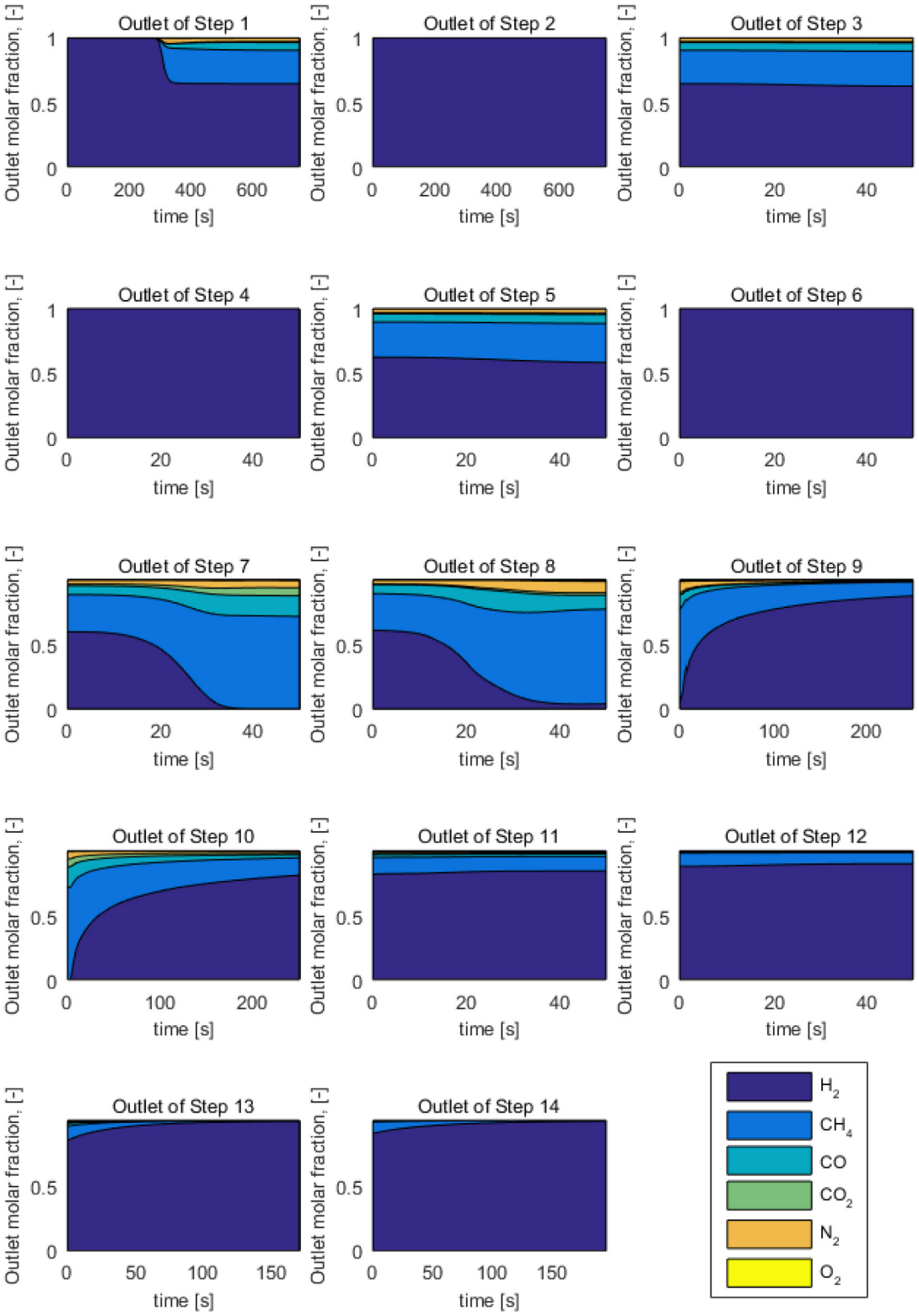

Fig. 8. Outlet gas phase concentrations from the bed over the step time during the PSA cycle. Steps: (1) AC Adsorption; (2) 13X Adsorption; (3) AC Evacuation; (4) 13X Evacuation; (5) AC Depressurising Pressure Equalisation; (6) 13X Depressurising Pressure Equalisation; (7) AC Blowdown; (8) 13X Blowdown; (9) 13X Purge; (10) AC Purge; (11) 13X Pressurising Pressure Equalisation; (12) AC Pressurising Pressure Equalisation; (13) AC Repressurisation; (14) 13X Repressurisation.

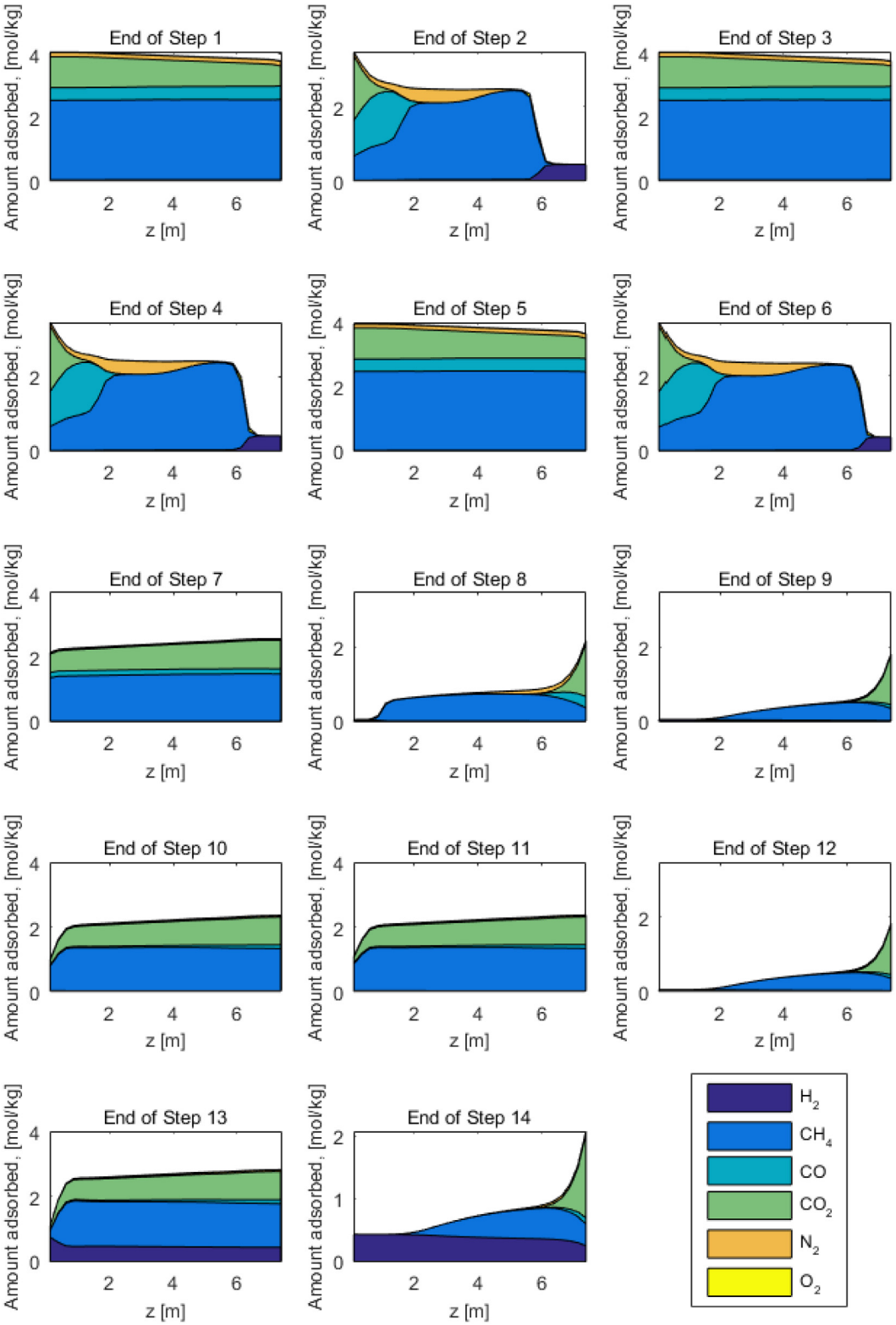

Fig. 9. Adsorbate loading at the end of each step during the PSA cycle. Steps: (1) AC Adsorption; (2) 13X Adsorption; (3) AC Evacuation; (4) 13X Evacuation; (5) AC Depressurising Pressure Equalisation; (6) 13X Depressurising Pressure Equalisation; (7) AC Blowdown; (8) 13X Blowdown; (9) 13X Purge; (10) AC Purge; (11) 13X Pressurising Pressure Equalisation; (12) AC Pressurising Pressure Equalisation; (13) AC Repressurisation; (14) 13X Repressurisation.

Table 5. Comparison of concentration levels of impurities in hydrogen product with the allowable concentration levels for mobility application.

Impurity	Allowable Concentration (ppm)	Impurities concentration in H_2 product (ppm)
Methane	2	1
Carbon monoxide	0.2	3×10^{-10}
Carbon dioxide	2	4×10^{-6}
Nitrogen	100	0.002
Oxygen	5	0.007

Table 6. An overview of the different streams involved the H_2 PSA process (Rep −repress; Evac −evacuation; BD −blowdown).

Conditions	Feed stream	Purge in stream	Rep (2 streams)	Product stream	Evac stream	BD stream I	BD stream II	Purged out stream
Composition (vol.)								
H_2	0.643	∼1	∼1	∼1	∼1	0.264	0.246	0.624
CH_4	0.257	–	–	–	–	0.528	0.546	0.269
CO	0.059	–	–	–	–	0.119	0.127	0.058
CO_2	0.013	–	–	–	–	0.035	0.014	0.024
N_2	0.026	–	–	–	–	0.047	0.063	0.022
$_{\cdot}O_2$	0.002	–	–	–	–	0.004	0.004	0.003
Pressure (bar)	30	1	30	30	25	1	1	1
Temperature (K)	298	298	298	307	306	303	303	286
Flow rate (mol/s)	30	10	16	23	15	71	101	16
Average cycle flow rate (mol/s/cycle)	16.07	1.8	2.2	12.54	0.55	2.4	3.5	2.92

Table 7. Specifications for activated carbon and zeolite columns.

Column specifications	Carbon column	Zeolite column
Length (L)	7.5 m	7.5 m
Outer Radius (r_{out})	0.355 m	0.355 m
Inner Radius (r_{in})	0.350 m	0.350 m
Volume of adsorbent needed (V)	1.15 m^3	1.15 m^3
Amount of adsorbent needed (m)	981 kg	1616 kg

Table 8. Performance parameters of the optimised PSA cycle.

Performance Parameters	Value
Purity [−]	99.999+%
Recovery [−]	78%
Productivity, [moles of H_2 per m^3 of adsorbent bed per second]	9.26
Compressor Energy Consumption, [kWh/kg of H_2 produced]	3.37

3% increase in the recovery of hydrogen product can be achieved using the PSA process if used as a reducing gas for the direct reduction of iron ore as interpreted from Figure 5.

Hence, from the multi-bed pressure swing adsorption model developed in the study, it is possible to produce high purity (>99.999 vol%) hydrogen product from coke oven gas at a recovery of over 75% with the strict quality requirements of the desired hydrogen fuel source for mobility application, as well for other internal steelmaking applications.

4 Conclusions

A flexible, fast and robust simulation tool for simulating a variety of pressure swing adsorption processes considering both equilibrium and kinetic effects using a detailed non-isothermal and non-isobaric model has been developed in the study. It has been successfully used for optimisation of a 14-step multi-bed PSA cycle for producing high purity hydrogen from coke oven gas. The model was optimized by performing several simulation tests to achieve high process performance in terms of purity (>99.999%) and recovery (>75%) of the H_2 product, productivity of the adsorbents and energy consumption for compression of gases. Also, the bottom product which is a methane rich stream could be used for its heating value to partially displace natural gas consumption in the internal operations of the industry. Thus, the concept developed in this study allows for an increased energy efficiency of coal usage by better utilisation of its by-product i.e., coke oven gas by converting it into valuable H_2 product.

Nomencluture

A	Cross-sectional area of the column [m^2]
c	Fluid phase concentration [$mol.m^{-3}$]
C_{pg}	Specific heat capacity of gas phase [$J.mol^{-1}.K^{-1}$]
C_{ps}	Specific heat capacity of adsorbent [$J.kg^{-1}.K^{-1}$]
C_{pw}	Specific heat capacity of wall [$J.kg^{-1}.K^{-1}$]
$D\text{-}_{ax}$	Axial mass dispersion co-efficient [$m^2.s^{-1}$]
D_m	Molecular diffusivity [$m^2.s^{-1}$]
D_k	Knudsen diffusivity [$m^2.s^{-1}$]
D_e	Effective diffusivity [$m^2.s^{-1}$]
E	Compressor energy consumption [J]
f	State variable [−]
f_m	Flow rate [$mol.s^{-1}$]
h	Heat transfer co-efficient [$J.m^{-2}.K^{-1}.s^{-1}$]
H	Enthalpy [$kJ.mol^{-1}$]
k	Mass transfer co-efficient [s^{-1}]
L	Column length [m]
MW	Molecular weight [$kg.mol^{-1}$]
N	Number of discretization volumes
P	Pressure [Pa]
Pr	Prandtl number
q	Solid phase concentration [$mol.m^{-3}$]
r	Column radius [m]
r_p	Particle radius [m]
r_{pore}	Pore radius [m]
R	Universal gas constant (=8.314) [$J.mol^{-1}.K^{-1}$]
Re	Reynolds number
S	Entropy [$kJ.mol^{-1}K^{-1}$]
Sc	Schmidt number
t	Time [s]
T	Temperature [K]
v	Interstitial velocity [$m.s^{-1}$]
V	Volume of cell [m^3]
y	Gas phase composition [−]
z	Axial co-ordinate [m]
ε	Bed porosity [−]
ε_p	Particle porosity [−]
ρ_g	Gas phase density [$mol.m^{-3}$]
ρ_s	Adsorbent density [$kg.m^{-3}$]
ρ_w	Wall density [$kg.m^{-3}$]
λ_{ax}	Axial thermal dispersion co-efficient [$J.m^{-1}.K^{-1}.s^{-1}$]
λ_g	Thermal conductivity of gas [$J.m^{-1}.K^{-1}.s^{-1}$]
λ_w	Thermal conductivity of wall [$J.m^{-1}.K^{-1}.s^{-1}$]
μ	Viscosity of fluid [Pa.s]
σ ξ	Lennard Jones potential energy function [−]
Ω	Collision integral [−]
τ	Tortuosity [−]
δ	small change ($=10^{-10}$)
τ	Dimensionless time [−]
γ	Adiabatic constant [−]
η	Compressor efficiency [−]

Acronyms

13X	Zeolite 13X
AC	Activated carbon
CSS	Cyclic steady state
LDF	Linear driving force

Subscripts

0	Non-dimensional reference value
a	Ambient
acc	Accumulated
ads	Adsorption
BD	Blowdown
Evac	Evacuation
H	High
i	Component
in	Inside
I	Intermediate/Evacuation
j	Cell index
L	Low
out	Outside
PEQ	Pressure Equalisation
Rep	Repress
w	Wall

Superscripts

*	Equilibrium condition
¯	Dimensionless term

References

1. T.W. Kienlen, The Future of Coal: Options for a carbon constrained world, MIT study on the future of coal, 10 (4), 5–16 (2007)
2. IEA, Key World Energy Statistics, OECD Publishing, 28–35 (2009)
3. J.M. Bermudez, A. Arenillas, R. Luque et al., An overview of novel technologies to valorise coke oven gas surplus, Fuel Process. Technol. 110, 150–159 (2013).
4. B. Ramani, Development of a dynamic multi-bed Pressure Swing Adsorption process for high purity hydrogen production

from Coke Oven Gas: A mathematical modeling approach, Repository, TU Delft, 1–110 (2016).
5. R. Razzaq, C. Li, S. Zhang, Coke oven gas: availability, properties, purification, and utilization in China, Fuel 113, 287–299 (2013)
6. Market Report: Hydrogen mobility – Today and into the future, M. Adams, 2023, <www.h2-view.com/story/market-report-hydrogen-mobility-today-and-into-the-future>
7. Linde Engineering, Hydrogen Recovery by Pressure Swing Adsorption, Linde, 4–8 (2010)
8. Y. P. Z. Oliver, Comparison of finite difference and finite volume methods & the Development of an educational tool for the Fixed bed gas adsorption problem, National University of Singapore, 10–36 (2011)
9. T. Lipman, An Overview of Hydrogen Production and Storage Systems with Renewable Hydrogen Case Studies, Clean Energy States Alliance, 12 (2011)
10. J.A. Delgado, V.I. Águeda, M.A. Uguina et al., Adsorption and diffusion of H_2, CO, CH_4, and CO_2 in BPL activated carbon and 13X zeolite: evaluation of performance in press ure swing adsorption hydrogen purification by simulation, Ind. Eng. Chem. Res. 53 (40), 15414–15426 (2014)
11. R. Yang, Gas Separation by Adsorption Processes. 2, 30–110 (1988)
12. Y. Park, D.K. Moon, Y.H. Kim et al., Adsorption isotherms of CO_2, CO, N_2, CH_4, Ar and H_2 on activated carbon and zeolite LiX up to 1.0 MPa, Adsorption 20 (4), 631–647 (2014)
13. G. Narin, V.F.D. Martins, M. Campo et al., Light olefins/paraffins separation with 13X zeolite binder less beads, Sep. Purif. Technol. 133, 452–475 (2014)
14. M.C. Georgiadis, J.R. Banga, E.N. Pistikopoulos, Process Systems Engineering: Dynamic Process Modelling. 7, 137–167 (2010)
15. M.B. Donald, Introduction to Chemical Engineering, Chemical Engineering Science. 6 (4–5), 235 (1957)
16. Y.J. Kim, Y.S. Nam, Y.T. Kang, Study on a numerical model and PSA (pressure swing adsorption) process experiment for CH_4/CO_2 separation from biogas, Energy 91, 732–741 (2015)
17. D. Nikolic, A. Giovanoglou, M.C. Georgiadis et al., Generic modelling framework for gas separations using multibed pressure swing adsorption processes, Ind. Eng. Chem. Res. 47 (9), 3156–3169 (2008)
18. R. Haghpanah, A. Majumder, R. Nilam, A. Rajendran, S. Farooq, I. a Karimi, M. Amanullah, Multi-objective Optimization of a 4-step Adsorption Process for Post-combustion CO2 Capture Using Finite Volume Technique, Ind. Eng. Chem. Res. 52, 4249–4265 (2013)
19. D. D. Do, Adsorption Analysis: Equilibria and Kinetics, Imperial College Press. 2, 389–391 (1998)
20. B.E. Poling, M. Prausnitz, J. P. O'Connell, The properties of gases and liquids, Library (Lond). 23 (3), 1–11 (2006)
21. L. I. Berger, M. Frenkel, C. A. Koh, P. E. Bradley, J. R. Fuhr, W. H. Koppenol, T. J. Bruno, Handbook of chemistry and physics, CRC Press. 95, 6–57 (2014)
22. P. Biswas, S. Agrawal, S. Sinha, Modelling and simulation for pressure swing adsorption system for hydrogen purification, Chem. Biochem. Eng. Q. 24 (4), 409–414 (2010)
23. National Physical Laboratory, New Methods for Hydrogen Purity Analysis, ISO 14687, 3–4 (2011)
24. J. M. Ohi, N. Vanderborgh, G. Voecks, Hydrogen Fuel Quality Specifications for Polymer Electrolyte Fuel Cells in Road Vehicles, Fuel Cell Technologies Office, U.S. Department of Energy, 2 (2016)
25. World first for steel: arcelorMittal investigates the industrial use of pure hydrogen, ArcelorMittal, 2019, <https://corporate.arcelormittal.com/media/news-articles/2019-mar-28-world-first-for-steel>.
26. F. Patisson, O. Mirgaux, Hydrogen ironmaking: how it works, Metals 10, 922 (2020)

Cite this article as: Balan Ramani, Jan van der Stel, Gerard Jagers, Wim Buijs, , Hydrogen production from coke oven gas using pressure swing adsorption process – a mathematical modelling approach, Matériaux & Techniques **111**, 205 (2023)